

RESEARCH

Online Acoustic System Identification Exploiting Kalman Filtering and an Adaptive Impulse Response Subspace Model

Thomas Haubner^{*}, Andreas Brendel and Walter Kellermann

Abstract

We introduce a novel algorithm for online estimation of acoustic impulse responses (AIRs) which allows for fast convergence by exploiting prior knowledge about the fundamental structure of AIRs. The proposed method assumes that the variability of AIRs of an acoustic scene is confined to a low-dimensional manifold which is embedded in a high-dimensional space of possible AIR estimates. We discuss various approaches to locally approximate the AIR manifold by affine subspaces which are assumed to be tangential hyperplanes to the manifold. The validity of these model assumptions is verified for simulated data. Subsequently, we describe how the learned models can be used to improve online AIR estimates by projecting them onto an adaptively estimated subspace. The parameters determining the subspace are learned from training samples in a local neighbourhood to the current AIR estimate. This allows the system identification algorithm to benefit from preceding estimates in the acoustic scene. To assess the proximity of training data AIRs to the current AIR estimate, we introduce a probabilistic extension of the Euclidean distance which improves the performance for applications with correlated excitation signals. Furthermore, we describe how model imperfections can be tackled by a soft projection of the AIR estimates. The proposed algorithm exhibits significantly faster convergence properties in comparison to a high-performance state-of-the-art algorithm. Furthermore, we show an improved steady-state performance for speech-excited system identification scenarios suffering from high-level interfering noise and nonunique solutions.

Keywords: Online Acoustic System Identification; Kalman Filter; Subspace Model; Adaptation Control

1 Introduction

The continuously increasing amount of acoustic communication devices has fueled the research on reliable speech enhancement algorithms. In this context system identification has proven to be a vital part of many state-of-the-art approaches [1, 2]. In particular online algorithms are required to cope with the large variety of acoustic environments devices are exposed to. However, even after decades of research [3, 4, 5, 6], Online Supervised Acoustic System Identification (OSASI)-based speech enhancement algorithms are significantly challenged by interfering noise signals and their limited convergence rate. In this paper we propose a method which tackles remaining limitations of modern OSASI algorithms.

Both convergence speed and noise-robustness are usually addressed by adaptive step size-controlled

adaptive filter (AF) algorithms [2]. Their performance decisively depends on the stochastic properties of the excitation and the noise signals [7]. In particular, for stationary white excitation signals a fast convergence speed and robust steady-state performance is achieved. This observation has led to a variety of excitation signal-dependent adaptive step size selection schemes with the most famous one being the power-normalization of the time-domain normalized least-mean-squares (NLMS) algorithm [7]. Its scalar time-domain step size has been extended to a frequency-dependent step size to cope with the temporal correlation of many excitation signals, i.e., speech or music [8]. In particular the frequency-dependent power normalization in block processing approaches led to computationally efficient and faster converging algorithms [4, 9]. The robustness against nonstationary interfering noise sources was initially addressed by binary adaptation control, i.e., stalling the filter adaptation whenever the noise power exceeds a predefined threshold [10]. The scalar and binary decision was later extended

^{*}Correspondence: thomas.haubner@fau.de

Multimedia Communications and Signal Processing,
Friedrich-Alexander-University Erlangen-Nürnberg (FAU), Cauerstr. 7,
91058, Erlangen, Germany.

Full list of author information is available at the end of the article.

to a frequency-dependent continuous step size control [11]. In particular the probabilistic inference of the step size by a Kalman Filter (KF) has shown great potential [12, 13, 14]. Yet, the KF performance decisively depends on an accurate estimate of the noise power spectral density (PSD) [15]. Here, significant performance improvements relative to classical PSD estimators have been achieved by modern machine-learning based approaches [16, 17]. Despite the improved noise robustness, these approaches still achieve only slow convergence speed for scenarios suffering from permanently low Signal-to-Noise-Ratio (SNR), e.g., as in driving cars with open windows.

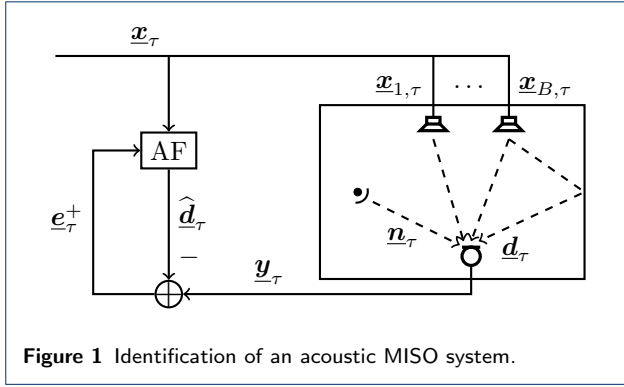
Recently, besides adaptation control, the exploitation of prior knowledge about the structure of acoustic impulse responses (AIRs) has been successfully used to deal with slow convergence and non-robust steady-state performance [18, 19, 20, 21]. These algorithms rely on the assumption that not all possible AIR estimates, i.e., Finite Impulse Response (FIR) filters of fixed length, are equally likely, i.e., certain regions exhibit a higher probability of representing a valid AIR. In [18] this assumption has been used by regularizing a least-squares system identification cost function with the Mahalanobis distance based on an estimated AIR covariance matrix. The extreme case that the AIRs of a considered acoustic scene can all be represented by a structured subset of the high-dimensional estimation space, i.e., FIR filters of fixed length, motivates the assumption of a low-dimensional AIR manifold [22]. Its existence is often tightly coupled to the parameter changes of an underlying physical process, e.g., location of sources and sensors or temperature changes, which govern the variability of the AIRs [23]. Noisy AIR estimates can be enhanced by projection onto the manifold, i.e., by removing the part which is not confined to the manifold. Yet due to the complex interaction of the physical parameters and the high-dimensional AIRs, an analytic manifold description is difficult to obtain. However, in many applications a device is exposed to a reoccurring acoustic scene which allows to collect AIR estimates. These estimates can serve as training data to optimize a data-driven AIR manifold model which OSASI algorithms can exploit for improved performance. Various approaches have been proposed to model an AIR manifold with the most prominent one being a global affine subspace whose parameters are estimated by Principal Component Analysis (PCA) [24]. However, due to the restrictive assumption that all AIRs are confined to a single affine subspace, this approach is limited to simplistic scenarios (cf. Sec. 3.4). In [19, 21] this model has been extended to a mixture of affine subspaces whose parameters are learned in advance by

clustering the AIRs followed by a PCA of each cluster. Due to the increased modelling capabilities, this local affine subspace approach can represent the AIRs of a larger class of acoustic scenes. However, its computational complexity increases significantly if the number of subspaces is increased to represent realistic acoustic scenes (cf. Sec. 3.4). Besides the affine subspace-based approaches, a globally nonlinear manifold model has been proposed in [20] and was used in an offline least-squares system identification task.

In this paper, we introduce a novel algorithm which exploits an adaptive AIR subspace model for enhancing KF-based system identification algorithms. For this we discuss various data-driven local manifold approximations by affine subspaces. The validity of the model assumptions is verified for simulated AIRs. For fusing the adaptive subspace model with the KF we suggest a novel probabilistic inference method to estimate the subspace parameters. Furthermore, we relax the idea of hard projecting a noisy AIR estimate onto the AIR manifold to a soft projection which allows the algorithm to cope with model imperfections. It is shown that the proposed method improves the convergence speed of KF-based system identification algorithms and achieves higher steady-state performance in scenarios suffering from high-level interfering noise. In addition, we show improved AF performance for system identification scenarios that are challenged by nonunique minimum mean square error (MMSE) solutions [25, 26]. This problem is often faced in rendering and teleconferencing applications for which the excitation signals are composed of less sources than loudspeakers.

In this paper, vectors are typeset as bold lowercase letters and matrices as bold uppercase letters with underlined symbols representing time-domain quantities. The all-zero matrix of dimension $D_1 \times D_2$ is denoted by $\mathbf{0}_{D_1 \times D_2}$, the $D \times D$ -dimensional identity matrix by \mathbf{I}_D and the Discrete Fourier Transform (DFT) matrix by \mathbf{F}_D , respectively. Transposition and Hermitian transposition are represented by $(\cdot)^T$ and $(\cdot)^H$. Furthermore, the i th element of a vector \mathbf{w} is denoted by $[\mathbf{w}]_i$ and the $\text{diag}(\cdot)$ operator creates a diagonal matrix from its vector-valued argument. Finally, equivalency of two terms up to a constant is denoted by $\stackrel{c}{=}$.

The remainder of this paper is structured as follows: In Sec. 2 a probabilistic signal observation model is introduced which relates the noisy observations to the unknown AIRs. Subsequently, in Sec. 3, various affine subspace approaches to locally model an AIR manifold are described and evaluated for simulated data. The fusion of the affine subspace models with a KF-based OSASI algorithm is introduced in Sec. 4. Experimental results for the proposed algorithm are shown in Sec. 5. Finally, the paper is concluded in Sec. 6.



2 Probabilistic Signal Model

We first introduce a probabilistic signal model for describing the microphone observations of a multiple-input single-output (MISO) system identification scenario with B loudspeakers and one microphone as depicted in Fig. 1.

A block of microphone observations at time index τ

$$\underline{y}_\tau = \underline{d}_\tau + \underline{n}_\tau \in \mathbb{R}^R \quad (1)$$

is modeled as a superposition of the noise-free observation vector \underline{d}_τ and the noise signal vector \underline{n}_τ . Each signal block, i.e., \underline{y}_τ , \underline{d}_τ , and \underline{n}_τ , contains R consecutive samples:

$$\underline{y}_\tau = [\underline{y}_{\tau R-R+1} \quad \underline{y}_{\tau R-R+2} \quad \dots \quad \underline{y}_{\tau R}]^T \in \mathbb{R}^R. \quad (2)$$

The noise-free observation \underline{d}_τ is modeled by a linear convolution of the AIRs $\underline{w}_{b,\tau} \in \mathbb{R}^L$ with $b \in \{1, \dots, B\}$ of length L with the respective loudspeaker signal blocks

$$\underline{x}_{b,\tau} = [\underline{x}_{b,\tau R-M+1} \quad \dots \quad \underline{x}_{b,\tau R}]^T \in \mathbb{R}^M \quad (3)$$

of length $M = R + L$ and subsequently adding up the B convolution products. This can be expressed efficiently in the DFT domain [27]

$$\underline{d}_\tau = \sum_{b=1}^B \mathbf{Q}_1^T \mathbf{F}_M^{-1} \mathbf{X}_{b,\tau} \mathbf{F}_M \mathbf{Q}_2 \underline{w}_{b,\tau}, \quad (4)$$

with the diagonal matrix $\mathbf{X}_{b,\tau} = \text{diag}(\mathbf{F}_M \underline{x}_{b,\tau})$, containing the DFT-domain loudspeaker signals of block τ , the constraint matrix $\mathbf{Q}_1^T = [\mathbf{0}_{R \times L} \quad \mathbf{I}_R]$ and the zero-padding matrix $\mathbf{Q}_2^T = [\mathbf{I}_L \quad \mathbf{0}_{L \times R}]$. By inserting the convolution model (4) into the additive signal model (1) and introducing the acoustic transfer functions (ATFs) $\underline{w}_{b,\tau} = \mathbf{F}_M \mathbf{Q}_2 \underline{w}_{b,\tau}$, we obtain the time-

domain observation model

$$\underline{y}_\tau = \sum_{b=1}^B \mathbf{Q}_1^T \mathbf{F}_M^{-1} \mathbf{X}_{b,\tau} \underline{w}_{b,\tau} + \underline{n}_\tau. \quad (5)$$

A corresponding frequency-domain observation model is computed by first zero-padding the signals in Eq. (5) and subsequently applying the DFT [27]:

$$\underline{y}_\tau = \mathbf{F}_M \mathbf{Q}_1 \underline{y}_\tau = \mathbf{C}_\tau \underline{w}_\tau + \underline{n}_\tau \in \mathbb{C}^M. \quad (6)$$

Here, we used the overlap-save constrained loudspeaker signal matrix

$$\mathbf{C}_\tau = [\mathbf{C}_{1,\tau} \quad \dots \quad \mathbf{C}_{B,\tau}] \in \mathbb{C}^{M \times BM} \quad (7)$$

with $\mathbf{C}_{b,\tau} = \mathbf{F}_M \mathbf{Q}_1 \mathbf{Q}_1^T \mathbf{F}_M^{-1} \mathbf{X}_{b,\tau} \in \mathbb{C}^{M \times M}$ and the MISO ATF vector

$$\underline{w}_\tau = [\underline{w}_{1,\tau}^T \quad \dots \quad \underline{w}_{B,\tau}^T]^T \in \mathbb{C}^{MB}. \quad (8)$$

Note that the corresponding time-domain AIR vector is obtained by

$$\underline{w}_\tau = \left(\mathbf{I}_B \otimes \left(\mathbf{Q}_2^T \mathbf{F}_M^{-1} \right) \right) \underline{w}_\tau \in \mathbb{R}^Q \quad (9)$$

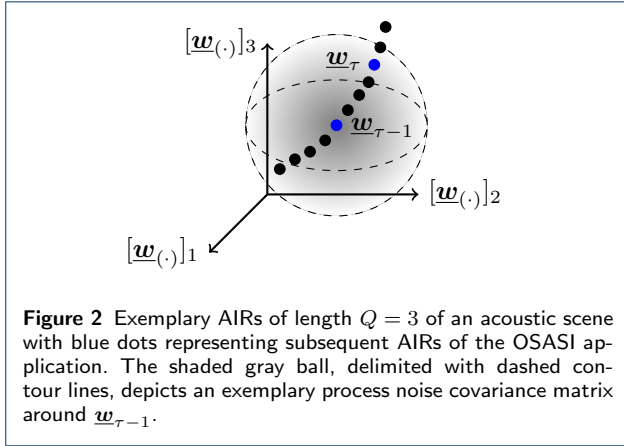
with $Q = LB$. The interfering noise term \underline{n}_τ is modeled as a proper complex zero-mean Gaussian random vector [27]

$$\underline{n}_\tau \sim \mathcal{N}_c(\underline{n}_\tau | \mathbf{0}_{M \times 1}, \mathbf{\Psi}_\tau^N), \quad (10)$$

with covariance matrix $\mathbf{\Psi}_\tau^N \in \mathbb{C}^{M \times M}$.

3 Analysis of Acoustic Impulse Responses

In the following sections, we discuss various approaches to model the neighbourhood of the unknown AIR vector $\underline{w}_\tau \in \mathbb{R}^Q$. We start by introducing the first-order Markov model assumption which is commonly used in KF-based system identification algorithms and discuss its limitations. Subsequently, we describe how these limitations can be mitigated by modeling an AIR manifold. Finally, we discuss various affine subspace-based approaches to locally approximate the manifold. Note that a straightforward extension of the subsequently described MISO AIR models to multiple-input multiple-output (MIMO) systems is obtained by stacking the respective MISO AIR vectors \underline{w}_τ to an extended vector [21].



3.1 Acoustic Impulse Response Manifold

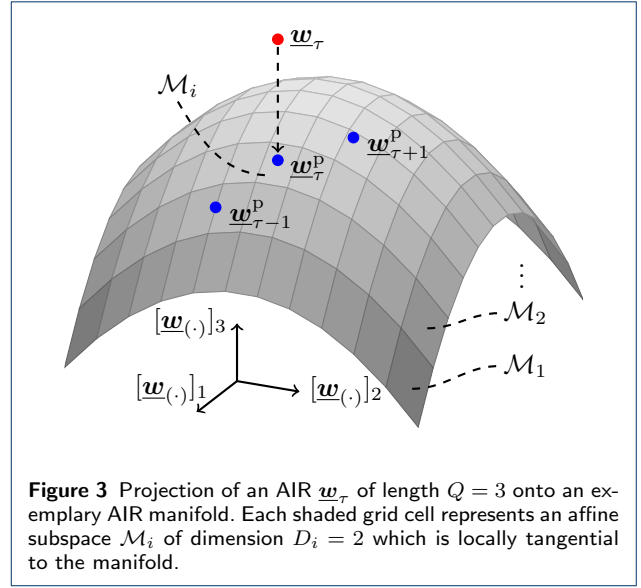
In [12, 27] it is suggested to describe the temporal propagation of the DFT-domain AIR vector \underline{w}_τ (cf. Eq. (9)) by a random walk Markov model

$$\begin{aligned} \underline{w}_\tau &= A \underline{w}_{\tau-1} + \Delta \underline{w}_\tau, \\ \Delta \underline{w}_\tau &\sim \mathcal{N}_c(\Delta \underline{w}_\tau | \mathbf{0}_{M \times 1}, \Psi_\tau^{\Delta W}) \end{aligned} \quad (11)$$

with the state transition coefficient A and the block-diagonal process noise covariance matrix

$$\Psi_\tau^{\Delta W} = \begin{bmatrix} \Psi_{11,\tau}^{\Delta W} & \cdots & \mathbf{0}_{M \times M} \\ \vdots & \ddots & \vdots \\ \mathbf{0}_{M \times M} & \cdots & \Psi_{BB,\tau}^{\Delta W} \end{bmatrix} \in \mathbb{C}^{BM \times BM}. \quad (12)$$

As depicted in Fig. 2, the random walk model describes a continuous temporal propagation of subsequent AIRs $\underline{w}_{\tau-1}$ and \underline{w}_τ , depicted as blue dots, of the OSASI application. However, as no additional knowledge about the filter coefficients is assumed, the process noise power is distributed into all directions of the high-dimensional FIR filter vector space \mathbb{R}^Q , as shown by the shaded gray area in Fig. 2. In contrast, the AIRs in the vicinity of $\underline{w}_{\tau-1} \in \mathbb{R}^Q$ often populate only a subset of this space [22]. This is visualized in Fig. 2 by showing exemplary samples of the surrounding AIR vectors as black dots. On a global view this motivates the assumption that all AIRs are confined to a structured subset of the vector space \mathbb{R}^Q which is termed AIR manifold. As manifolds are locally Euclidean [28], each neighbourhood of an AIR can be described by an affine subspace \mathcal{M}_i of the vector space \mathbb{R}^Q . This is visualized in Fig. 3 where each shaded grid cell illustrates a different affine subspace \mathcal{M}_i . We now introduce a mathematical description of a single affine subspace which will serve as a basis for the following approaches to describe the manifold globally by patches of affine subspaces.



3.2 Affine Subspace Model

An affine subspace \mathcal{M}_i of dimension D_i is defined by:

$$\mathcal{M}_i := \{\underline{w}_\tau^p \in \mathbb{R}^Q | \underline{w}_\tau^p = \underline{\bar{w}}_i + \underline{V}_i \underline{\beta}_\tau, \underline{\beta}_\tau \in \mathbb{R}^{D_i}\}. \quad (13)$$

It is parametrized by its offset $\underline{\bar{w}}_i \in \mathbb{R}^Q$ and its basis matrix $\underline{V}_i \in \mathbb{R}^{Q \times D_i}$. The vector $\underline{\beta}_\tau$ represents the coordinates of the affine subspace element \underline{w}_τ^p in the basis spanned by the columns of \underline{V}_i .

An orthogonal projection of an arbitrary AIR vector $\underline{w}_\tau \in \mathbb{R}^Q$ onto the affine subspace \mathcal{M}_i is given by the linear mapping [29]

$$\underline{w}_\tau^p = f_{\mathcal{M}_i}(\underline{w}_\tau) = \underline{\bar{w}}_i + \underline{L}_i (\underline{w}_\tau - \underline{\bar{w}}_i) \in \mathbb{R}^Q \quad (14)$$

with the rank- D_i projection matrix

$$\underline{L}_i = \underline{V}_i (\underline{V}_i^T \underline{V}_i)^{-1} \underline{V}_i^T \in \mathbb{R}^{Q \times Q}. \quad (15)$$

Here, it is assumed that the columns in \underline{V}_i are linearly independent. Fig. 3 shows the projection of the AIR vector \underline{w}_τ onto an exemplary AIR manifold which is locally represented by the affine subspace \mathcal{M}_i .

3.3 Affine Subspace Parameter Estimation

We now discuss how to estimate the parameters of a single affine subspace \mathcal{M}_i , i.e., its offset $\underline{\bar{w}}_i$ and basis matrix \underline{V}_i , from a local training data set \mathcal{U}_i including K_i AIR vectors $\underline{w}_\kappa^{\text{tr}}$. We assume that the K_i samples of the local training data set \mathcal{U}_i form a subset of the full training data set \mathcal{U} , i.e., $\mathcal{U}_i \subseteq \mathcal{U}$, consisting of K samples in total. The indicator variable

$$z_{\kappa i} := \begin{cases} 1 & \text{if } \underline{w}_\kappa^{\text{tr}} \in \mathcal{U}_i, \\ 0 & \text{if } \underline{w}_\kappa^{\text{tr}} \notin \mathcal{U}_i \end{cases} \quad (16)$$

describes the assignment of the training samples to the local training data subsets. The offset of the affine subspace \mathcal{M}_i is estimated as arithmetic average of the local training data:

$$\bar{\mathbf{w}}_i = \frac{1}{K_i} \sum_{\kappa=1}^K z_{\kappa i} \mathbf{w}_{\kappa}^{\text{tr}} \quad (17)$$

with $K_i = \sum_{\kappa=1}^K z_{\kappa i}$. For computing the basis matrix \mathbf{V}_i we first estimate the local AIR covariance matrix

$$\mathbf{R}_i = \frac{1}{K_i - 1} \sum_{\kappa=1}^K z_{\kappa i} (\mathbf{w}_{\kappa}^{\text{tr}} - \bar{\mathbf{w}}_i)(\mathbf{w}_{\kappa}^{\text{tr}} - \bar{\mathbf{w}}_i)^T. \quad (18)$$

Subsequently, the basis matrix \mathbf{V}_i is determined by the eigenvectors corresponding to the D_i largest eigenvalues. Note that, due to the broadband nature of the AIR vector (9), the covariance matrix \mathbf{R}_i describes the correlation between different AIRs, i.e., $\mathbf{w}_{1,\tau}, \dots, \mathbf{w}_{B,\tau}$ as well as the correlation of different taps of one AIR $\mathbf{w}_{b,\tau}$. We now discuss how the number of affine subspaces I and the selection of the indicator variables $z_{\kappa i}$ results in different approaches to approximate the AIR manifold.

3.4 Local Training Data Estimation

In [21] it is proposed to cluster the training data into I disjoint local data sets \mathcal{U}_i by the k-means algorithm [30, 31]. Subsequently, each local training data set \mathcal{U}_i is used to compute a local affine subspace \mathcal{M}_i by the method described in Sec. 3.3. Note that the classical global PCA approach is contained as a special case with $I = 1$. We now evaluate the validity of this model for a typical MISO acoustic rendering scenario. The simulation parameters are summarized in Sec. 5 and the models are learned from $K = 5000$ training data samples. As evaluation measure we use the logarithmic system mismatch

$$\Upsilon_{\tau} = 10 \log_{10} \left(\frac{1}{B} \sum_{b=1}^B \frac{\|\mathbf{w}_{b,\tau} - \mathbf{Q}_3 \hat{\mathbf{w}}_{b,\tau}^{\text{p}}\|^2}{\|\mathbf{w}_{b,\tau}\|^2} \right) \quad (19)$$

of the true AIRs $\mathbf{w}_{b,\tau} \in \mathbb{R}^W$ of length $W \geq L$ and the projections of its first L taps $\hat{\mathbf{w}}_{b,\tau}^{\text{p}} \in \mathbb{R}^L$ onto the respective affine subspace model. Note that the zero-padding matrix $\mathbf{Q}_3^T = [\mathbf{I}_L \quad \mathbf{0}_{L \times W-L}] \in \mathbb{R}^{L \times W}$ ensures equal lengths of the true AIR vector and its truncated projection. Fig. 4 shows the average system mismatch $\bar{\Upsilon}$ which results from the projection of 500 ground-truth AIR vectors \mathbf{w}_{τ} onto the global affine subspace model (*Global Proj.* ($I = 1$)) and a mixture model with $I = 40$ clusters (*Mixture Proj.* ($I = 40$)) in

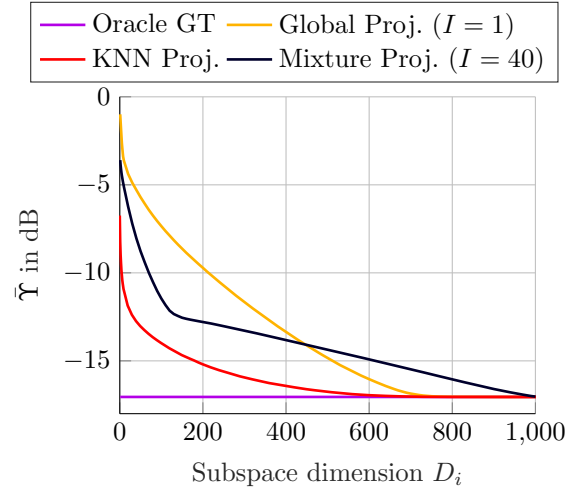


Figure 4 Average system mismatch $\bar{\Upsilon}$ of projecting 500 ground-truth MISO AIR vectors $\mathbf{w}_{\tau} \in \mathbb{R}^{BW}$ onto various affine subspace models ($B = 2$, $W = 4096$, $L = 512$). The subspace dimension $D_i = 0$ corresponds to using only the offset vector of the model as projected AIR.

dependence of the subspace dimension D_i . Note that for the mixture model the affine subspace with the lowest system mismatch Υ_{τ} is selected. In addition a benchmark, *Oracle GT*, is evaluated which represents the optimum choice for a length- L FIR filter representation by using the first L samples of the ground-truth AIRs, i.e., $\hat{\mathbf{w}}_{b,\tau}^{\text{p}} = \mathbf{Q}_3^T \mathbf{w}_{b,\tau}$. We conclude from Fig. 4 that for the considered scenario the global affine subspace assumption holds only coarsely. Due to the high variability of the AIRs representing the acoustic scene, a large subspace dimension is required to attain a reasonable average system mismatch $\bar{\Upsilon}$. This limits the denoising capability of the respective projection (cf. Sec. 4.3). In contrast, the mixture approach attains for small subspace dimensions D_i already a much lower average system mismatch $\bar{\Upsilon}$. However, as the affine subspaces \mathcal{M}_i are only representative for samples close to the offset vector $\bar{\mathbf{w}}_i$, its modeling capability depends decisively on the number of clusters I . This limitation can be mitigated by using more clusters. In the extreme case of using the same number of clusters as training data samples, i.e., $I = K$, each test sample is approximated by the best fitting nearest neighbour (NN) training sample. Motivated by the property of manifolds being locally Euclidean, the squared Euclidean distance

$$d_{\text{euc}}(\mathbf{w}_{\tau}, \mathbf{w}_{\kappa}^{\text{tr}}) = \|\mathbf{w}_{\tau} - \mathbf{w}_{\kappa}^{\text{tr}}\|^2 \quad (20)$$

in between the ground-truth AIR vector \mathbf{w}_{τ} and the training data samples $\mathbf{w}_{\kappa}^{\text{tr}}$ is used to select the NNs.

The respective NN approximation attains an average system mismatch of $\bar{Y} = -6.7$ dB (cf. *k-nearest neighbour (KNN) Proj.* at subspace dimension $D_i = 0$ in Fig. 4). We suspect that the NN model generalizes poorly to AIRs in between the training samples as the respective subspace is zero-dimensional, i.e., condensed to a single element. To remedy this limitation we suggest to remove the condition of non-overlapping local training data sets \mathcal{U}_i as used in [21]. In particular we propose to estimate the affine subspace parameters from the K_τ NN training samples $\mathbf{w}_\kappa^{\text{tr}}$ to the current ground-truth AIR vector \mathbf{w}_τ . Note that we index the subspace-related parameters by τ in the following to stress the dependence on the ground-truth AIR vector. The corresponding projection suggests a reconstruction of \mathbf{w}_τ from its surrounding K_τ training samples. Note that if the subspace dimension is chosen as $D_\tau = K_\tau - 1$, with K_τ being the number of neighbours, the projection can be computed directly from the training samples (*KNN Proj.*) as shown in the sequel. Note that one degree of freedom is required for computing the local offset vector $\bar{\mathbf{w}}_\tau$ (cf. Eq. (15)). The projection matrix \mathbf{L}_τ is obtained without eigenvalue decomposition of the local covariance matrix by choosing

$$\mathbf{V}_\tau = [\mathbf{w}_1^{\text{tr}} - \bar{\mathbf{w}}_\tau \quad \dots \quad \mathbf{w}_{K_\tau-1}^{\text{tr}} - \bar{\mathbf{w}}_\tau] \quad (21)$$

in Eq. (15). The corresponding *KNN Proj.* algorithm is evaluated in Fig. 4. The respective K_τ training AIRs are computed based on the squared Euclidean distance (20) w.r.t. the true AIR. We observe that, for an equivalent subspace dimension $D_i = D_\tau$, the proposed method achieves a much lower average system mismatch \bar{Y} in comparison to both the global and the mixture approach. Furthermore, due to removing the condition of disjoint local training data sets, the KNN-based projection achieves the benchmark performance (cf. *Oracle GT*) at a much lower subspace dimension in comparison to the mixture approach (cf. *Mixture Proj.*). This property is beneficial as the orthogonal space to the affine subspace is treated as noisy part of an AF estimate in the following (cf. Sec. 4.3).

4 Acoustic Impulse Response Denoising

In this section, we introduce the proposed OSASI algorithm which fuses a state-of-the-art KF adaptation with an adaptive AIR subspace model. The subspace parameters are estimated from the NN training samples (cf. Sec. 3.4). For computing the closest neighbours we propose a novel distance which takes the state uncertainty of the KF into account. Finally, we describe a probabilistically motivated frequency-dependent convex combination of the KF estimate and its projection onto the affine subspace which improves the performance of the baseline KF.

4.1 Kalman Filter-based Acoustic Impulse Response Estimation

The DFT-domain KF [12, 27] approach to OSASI suggests a probabilistic inference of the latent ATF vector \mathbf{w}_τ . For this, the conditional Probability Density Function (PDF) of \mathbf{w}_τ , given the current and the preceding observations $\mathbf{Y}_{1:\tau} = [\mathbf{y}_1, \dots, \mathbf{y}_\tau]$, is modeled by [27]

$$p(\mathbf{w}_\tau | \mathbf{Y}_{1:\tau}) = \mathcal{N}_c(\mathbf{w}_\tau | \hat{\mathbf{w}}_\tau^{\text{kf}}, \mathbf{P}_\tau) \quad (22)$$

with the ATF mean vector

$$\hat{\mathbf{w}}_\tau^{\text{kf}} = \left[\left(\hat{\mathbf{w}}_{1,\tau}^{\text{kf}} \right)^T \quad \dots \quad \left(\hat{\mathbf{w}}_{B,\tau}^{\text{kf}} \right)^T \right]^T \in \mathbb{C}^{MB} \quad (23)$$

and the state uncertainty matrix

$$\mathbf{P}_\tau = \begin{bmatrix} \mathbf{P}_{11,\tau} & \dots & \mathbf{P}_{1B,\tau} \\ \vdots & \ddots & \vdots \\ \mathbf{P}_{B1,\tau} & \dots & \mathbf{P}_{BB,\tau} \end{bmatrix} \in \mathbb{C}^{BM \times BM}. \quad (24)$$

Due to the linear Gaussian DFT-domain state transition model (11) and observation model (6), a closed form recursive update of the likelihood (22) is given by the KF equations [32]. In particular by assuming a diagonal structure for the submatrices $\mathbf{P}_{ij,\tau}$ ($i, j \in \{1, \dots, B\}$) of the state uncertainty matrix \mathbf{P}_τ computationally efficient update rules are obtained [27]:

$$\mathbf{e}_\tau^+ = \mathbf{y}_\tau - \mathbf{C}_\tau \hat{\mathbf{w}}_{\tau-1}^{\text{kf}} \approx \mathbf{y}_\tau - \mathbf{A} \mathbf{C}_\tau \hat{\mathbf{w}}_{\tau-1}^{\text{kf}} \quad (25)$$

$$\mathbf{P}_{ij,\tau-1}^+ = \mathbf{A}^2 \mathbf{P}_{ij,\tau-1} + \Psi_{ij,\tau}^{\Delta \text{W}} \quad (26)$$

$$\mathbf{D}_\tau = \sum_{i,j=1}^B \mathbf{X}_{i,\tau} \mathbf{P}_{ij,\tau-1}^+ \mathbf{X}_{j,\tau}^H + \frac{M}{R} \Psi_\tau^{\text{N}} \quad (27)$$

$$\mathbf{\Lambda}_{i,\tau} = \sum_{j=1}^B \left(\mathbf{P}_{ij,\tau-1}^+ \mathbf{X}_{j,\tau}^H \right) \mathbf{D}_\tau^{-1} \quad (28)$$

$$\hat{\mathbf{w}}_{i,\tau}^{\text{kf}} = \hat{\mathbf{w}}_{i,\tau-1}^{\text{kf}} + \mathbf{G} \mathbf{\Lambda}_{i,\tau} \mathbf{e}_\tau^+ \quad (29)$$

$$\mathbf{P}_{ij,\tau} = \mathbf{P}_{ij,\tau-1}^+ - \frac{R}{M} \mathbf{K}_{i,\tau} \sum_{l=1}^B \mathbf{X}_{l,\tau} \mathbf{P}_{lj,\tau-1}^+. \quad (30)$$

Note that, in contrast to [27], we introduced a gradient constraint matrix $\mathbf{G} = \mathbf{F}_M \mathbf{Q}_2 \mathbf{Q}_2^T \mathbf{F}_M^{-1}$ to ensure a zero-padded time-domain AIR vector [33] and set the state transition factor \mathbf{A} to one in the prior error computation (25) [6]. The resulting update rules (25) - (30) can be interpreted as an extension of the classical Frequency-Domain Adaptive Filter (FDAF)

[7] to multiple excitation signals including an adaptive frequency-dependent step size embedded in the Kalman gain matrix $\mathbf{\Lambda}_{i,\tau}$.

The required process and observation noise covariance matrices

$$\mathbf{\Psi}_\tau^{\Delta W} = (1 - A^2) \mathbf{\Psi}_\tau^W \quad (31)$$

$$\mathbf{\Psi}_\tau^N = \lambda_N \mathbf{\Psi}_{\tau-1}^N + (1 - \lambda_N) \mathbf{e}_\tau^+ (\mathbf{e}_\tau^+)^H \quad (32)$$

are estimated from the observed microphone signals using the estimated ATF power

$$\mathbf{\Psi}_\tau^W = \lambda_W \mathbf{\Psi}_{\tau-1}^W + (1 - \lambda_W) \hat{\mathbf{w}}_{\tau-1}^{\text{kf}} (\hat{\mathbf{w}}_{\tau-1}^{\text{kf}})^H \quad (33)$$

and the recursive averaging factors λ_W and λ_N [6, 15, 34].

4.2 Adaptive Subspace Tracking

In Sec. 3.4 we described the idea of learning an affine subspace \mathcal{M}_τ for the current test sample \mathbf{w}_τ from the surrounding K_τ NNs in the training data. This approach is straightforwardly extended to the OSASI application by computing the affine subspace \mathcal{M}_τ based on the NNs w.r.t to the current AF estimate $\hat{\mathbf{w}}_\tau^{\text{kf}}$ (cf. Eq. (22)). We now discuss the question if there are better choices than the simple squared Euclidean distance (20) for computing the closest neighbours in the training data set. For this we exploit the probabilistic KF model (22) which renders an uncertainty measure \mathbf{P}_τ of the current mean estimate $\hat{\mathbf{w}}_\tau^{\text{kf}}$. We suggest the negated likelihood of the training data samples given the KF estimate (cf. Eq. 22) as squared distance measure

$$-\log p(\mathbf{w}_\kappa^{\text{tr}} | \mathbf{Y}_{1:\tau}) \quad (34)$$

$$= -\log \mathcal{N}_c(\mathbf{w}_\kappa^{\text{tr}} | \hat{\mathbf{w}}_\tau^{\text{kf}}, \mathbf{P}_\tau) \quad (35)$$

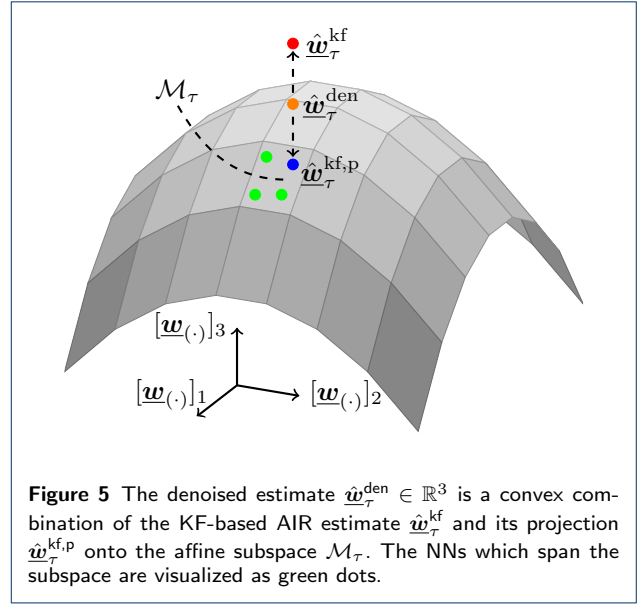
$$\stackrel{c}{=} (\mathbf{w}_\kappa^{\text{tr}} - \hat{\mathbf{w}}_\tau^{\text{kf}})^H \mathbf{P}_\tau^{-1} (\mathbf{w}_\kappa^{\text{tr}} - \hat{\mathbf{w}}_\tau^{\text{kf}}) \quad (36)$$

$$= d_{\text{kf}}(\mathbf{w}_\kappa^{\text{tr}}, \hat{\mathbf{w}}_\tau^{\text{kf}}). \quad (37)$$

Eq. (37) describes a frequency-dependent weighted squared Euclidean distance for which more reliable estimates, i.e., those having a lower state uncertainty, are more important, i.e., have a higher weight. Note that if the state uncertainty matrix \mathbf{P}_τ is chosen as identity matrix, as usually done in classical AF algorithms, the probabilistic distance measure (37) simplifies to the squared Euclidean distance (20).

4.3 Soft Subspace Projection

In Sec. 3 the local affine subspace approximation of an AIR manifold has been evaluated by the average system mismatch which results from a projection of a



noise-free AIR vector \mathbf{w}_τ onto a local affine subspace. Here, the projective mapping (14) sets the coordinates with little influence on the AIR vector to zero, i.e., yields a compressed description of the AIR vectors. This observation can now be exploited to denoise an AF estimate $\hat{\mathbf{w}}_\tau^{\text{kf}}$ by

$$\hat{\mathbf{w}}_\tau^{\text{kf,p}} = (\mathbf{I} \otimes (\mathbf{F}_M \mathbf{Q}_2)) f_{\mathcal{M}_\tau}(\hat{\mathbf{w}}_\tau^{\text{kf}}) \quad (38)$$

with the time-domain AF estimate

$$\hat{\mathbf{w}}_\tau^{\text{kf}} = \left(\mathbf{I} \otimes (\mathbf{Q}_2^T \mathbf{F}_M^{-1}) \right) \hat{\mathbf{w}}_\tau^{\text{kf}} \in \mathbb{R}^Q. \quad (39)$$

This projection removes all components of the KF-based AIR estimate $\hat{\mathbf{w}}_\tau^{\text{kf}}$ which are not supported by the surrounding training data samples spanning the affine subspace \mathcal{M}_τ . This is visualized in Fig. 5.

However, the experiments in Sec. 3 showed also the imperfection of the local affine subspace models as ground-truth AIRs could not be perfectly reconstructed by the projection. This motivates the idea of modelling an uncertainty measure around the manifold, i.e., diluting the deterministic model. We suggest to model this uncertainty by a proper complex Gaussian PDF

$$p(\mathbf{w}_\tau | \mathcal{M}_\tau) = \mathcal{N}_c(\mathbf{w}_\tau | \hat{\mathbf{w}}_\tau^{\text{kf,p}}, \mathbf{\Psi}_{\mathcal{M}_\tau}) \quad (40)$$

with the mean vector $\hat{\mathbf{w}}_\tau^{\text{kf,p}}$ being the projection of $\hat{\mathbf{w}}_\tau^{\text{kf}}$ onto the manifold and the covariance matrix $\mathbf{\Psi}_{\mathcal{M}_\tau} \in \mathbb{C}^{MB \times MB}$ expressing the uncertainty of the projection. Subsequently, the probability of the ATF

vector \mathbf{w}_τ given the KF likelihood (22) and the probabilistic manifold model (40) is given by

$$p(\mathbf{w}_\tau | \mathbf{Y}_{1:\tau}, \mathcal{M}_\tau) = \quad (41)$$

$$\mathcal{N}_c(\mathbf{w}_\tau | \hat{\mathbf{w}}_\tau^{\text{kf}}, \mathbf{P}_\tau) \mathcal{N}_c(\mathbf{w}_\tau | \hat{\mathbf{w}}_\tau^{\text{kf,p}}, \Psi_{\mathcal{M}_\tau}) \quad (42)$$

assuming $p(\mathbf{w}_\tau | \mathbf{Y}_{1:\tau}, \mathcal{M}_\tau) = p(\mathbf{w}_\tau | \mathbf{Y}_{1:\tau}) p(\mathbf{w}_\tau | \mathcal{M}_\tau)$. The Maximum-Likelihood (ML) estimate of \mathbf{w}_τ based on (42) is given by [35]:

$$\hat{\mathbf{w}}_\tau^{\text{den}} = (\mathbf{P}_\tau^{-1} + \Psi_{\mathcal{M}_\tau}^{-1})^{-1} (\mathbf{P}_\tau^{-1} \hat{\mathbf{w}}_\tau^{\text{kf}} + \Psi_{\mathcal{M}_\tau}^{-1} \hat{\mathbf{w}}_\tau^{\text{kf,p}}). \quad (43)$$

If the KF state uncertainty matrix \mathbf{P}_τ and the prior covariance matrix $\Psi_{\mathcal{M}_\tau}$ are assumed to be diagonal, Eq. (43) simplifies to

$$[\hat{\mathbf{w}}_{b,\tau}^{\text{den}}]_f = (1 - \alpha_{b,\tau,f}) [\hat{\mathbf{w}}_{b,\tau}^{\text{kf}}]_f + \alpha_{b,\tau,f} [\hat{\mathbf{w}}_{b,\tau}^{\text{kf,p}}]_f \quad (44)$$

with the ATF index b , the frequency bin index f and the convex combination weight

$$\alpha_{b,\tau,f} = \frac{[\mathbf{P}_{bb,\tau}]_{ff}}{[\mathbf{P}_{bb,\tau}]_{ff} + [\Psi_{\mathcal{M}_\tau,bb}]_{ff}}. \quad (45)$$

Here, the b th block diagonal element of $\Psi_{\mathcal{M}_\tau}$ is denoted by $\Psi_{\mathcal{M}_\tau,bb} \in \mathbb{C}^{M \times M}$. Eq. (44) represents a frequency-dependent convex combination of the KF estimate $\hat{\mathbf{w}}_\tau^{\text{kf}}$ and its projection $\hat{\mathbf{w}}_\tau^{\text{kf,p}}$ onto the manifold which is visualized in Fig. 5. The proposed approach favours the KF estimate $\hat{\mathbf{w}}_\tau^{\text{kf}}$ whenever the KF state uncertainty \mathbf{P}_τ is smaller than the prior model uncertainty $\Psi_{\mathcal{M}_\tau}$ and vice versa.

We will conclude this section by proposing a model for the prior uncertainty $\Psi_{\mathcal{M}_\tau}$. It is assumed that the model uncertainty

$$\Psi_{\mathcal{M}_\tau} = \frac{\beta_{\text{pr}}}{1 - A^2} \Psi_\tau^{\Delta W} \quad (46)$$

is a scaled version of the process noise covariance matrix $\Psi_\tau^{\Delta W}$ in the Markov model (11) with $\beta_{\text{pr}} > 0$ being a hyperparameter. This is motivated by the intrinsic ATF variability which is assumed to be proportional to the process noise power.

4.4 Algorithmic Description

Alg. 1 provides a detailed algorithmic description of the proposed KF with an Adaptive Subspace Projection (KF-ASP) algorithm for OSASI. For each block of microphone observations \mathbf{y}_τ and loudspeaker excitations \mathbf{x}_τ , the prior error \mathbf{e}_τ^+ is computed by using the ATF estimate of the previous time step $\hat{\mathbf{w}}_{\tau-1}^{\text{kf}}$

Algorithm 1 Proposed KF-ASP-based AIR estimation for one signal block \mathbf{y}_τ .

Compute prior error \mathbf{e}_τ^+ by Eq. (25)
 Estimate $\Psi_\tau^{\Delta W}$ and Ψ_τ^N by Eqs. (31)-(33).
 Update $\hat{\mathbf{w}}_\tau^{\text{kf}}$ and \mathbf{P}_τ by Eqs. (26)-(30)
 Compute NN training samples by distance metric $d_{(\cdot)}(\cdot, \cdot)$
 Compute subspace offset $\underline{\mathbf{w}}_\tau$ by Eq. (17)
 Compute projection matrix $\underline{\mathbf{L}}_\tau$ by Eq. (15)
 Project KF estimate onto affine subspace \mathcal{M}_τ by Eq. (14)
 Compute convex combination weights $\alpha_{b,\tau,f}$ by Eq. (45)
 Compute denoised KF estimate $\hat{\mathbf{w}}_\tau^{\text{den}}$ by Eq. (44)
 Assign denoised estimate to KF: $\hat{\mathbf{w}}_\tau^{\text{kf}} \leftarrow \hat{\mathbf{w}}_\tau^{\text{den}}$

(cf. Eq. (25)). Subsequently, the process noise and observation noise covariance matrices $\Psi_\tau^{\Delta W}$ and Ψ_τ^N are updated by Eqs. (31) - (33). Note that for computational efficiency only the diagonal elements are updated to ensure the submatrix diagonality of the state uncertainty matrix \mathbf{P}_τ (cf. Eq. (30)). Afterwards, the posterior mean vector $\hat{\mathbf{w}}_\tau^{\text{kf}}$ and the state uncertainty matrix \mathbf{P}_τ are updated by the KF Eqs. (26)-(30). The K_τ NNs to the posterior mean vector $\hat{\mathbf{w}}_\tau^{\text{kf}}$ are computed by the respective distance metric, i.e., $d_{\text{euc}}(\cdot, \cdot)$ or $d_{\text{kf}}(\cdot, \cdot)$ (cf. Eqs. (20), (37)). For an efficient computation of the inverse in Eq. (36), we only use the elements of the main diagonal of the state uncertainty matrix \mathbf{P}_τ . This reduces the computation of a full matrix inverse to a element-wise scalar inversion. The corresponding K_τ closest samples w.r.t. d_{euc} or d_{kf} are used as local training data set \mathcal{U}_τ to compute the associated subspace offset $\underline{\mathbf{w}}_\tau$ and projection matrix $\underline{\mathbf{L}}_\tau$ by Eqs. (17) and (15), respectively. Because of the chosen subspace dimension $D_\tau = K_\tau - 1$, the basis matrix $\underline{\mathbf{V}}_\tau$ Eq. (21) can be used in Eq. (15). The KF estimate $\hat{\mathbf{w}}_\tau^{\text{kf}}$ is then projected onto the affine subspace \mathcal{M}_τ by Eq. (14). Subsequently, the convex combination weights $\alpha_{b,\tau,f}$ (cf. Eq. (45)) are used to fuse the KF estimate $\hat{\mathbf{w}}_\tau^{\text{kf}}$ and its projection $\hat{\mathbf{w}}_\tau^{\text{kf,p}}$. Finally, the respective denoised estimated filter vector $\hat{\mathbf{w}}_\tau^{\text{den}}$ is used as posterior mean vector $\hat{\mathbf{w}}_\tau^{\text{kf}}$ of the KF.

5 Experiments

We now evaluate the proposed algorithm for a typical MISO acoustic system identification scenario. The acoustic scene is characterized by a loudspeaker array comprising $B = 2$ elements with a spacing of 10 cm and a single microphone. Loudspeakers and microphone are located in a room of dimensions [6 m, 5 m, 3.5 m] and a reverberation time of $T_{60} = 0.3$ s. While the position of the loudspeaker array is kept fixed at [3.0 m, 2.0 m, 1.2 m], the microphone position varies in a volumetric segment of a sphere with a radius in the range of $r \in [1.2 \text{ m}, 1.4 \text{ m}]$, an azimuthal angular range $\theta \in [45^\circ, 135^\circ]$ and elevation angle in the

range of $\phi \in [-5^\circ, 40^\circ]$ relative to the center of the loudspeaker array. All AIRs of length $W = 4096$ have been simulated using the image method [36, 37] with a maximum reflection order and a sampling frequency of $f_s = 8$ kHz. For each experiment the noise-free observation \underline{d}_τ is simulated by convolving the AIRs in \underline{w}_τ , corresponding to a random observation position in the sphere segment, with a randomly chosen excitation signal \underline{x}_τ . Here, we consider two types of excitation signals: spatially uncorrelated stationary white Gaussian noise (WGN) and speech. The speech signals are taken from a subset of the UWNU database [38] which comprises 15 different speakers. For the speech-excited scenarios we consider in addition to playing independent speech signals at each loudspeaker also a teleconferencing setup with strong correlation between the loudspeaker signals. The additive noise signal \underline{n}_τ is composed of an interfering WGN component $\underline{n}_{\text{wgn},\tau}$ and a nonstationary speech component $\underline{n}_{\text{sp},\tau}$, i.e., $\underline{n}_\tau = \underline{n}_{\text{wgn},\tau} + \underline{n}_{\text{sp},\tau}$. The variances of the noise signals $\underline{n}_{\text{wgn},\tau}$ and $\underline{n}_{\text{sp},\tau}$ are prescribed by SNR_{wgn} and SNR_{sp} , respectively. The set of interfering speech signals consists of 15 additional talkers from [38].

To evaluate the performance of the proposed algorithm we use the system mismatch Υ_τ (cf. Eq. (19)) and the Echo Return Loss Enhancement (ERLE)

$$\mathcal{E}_\tau = 10 \log_{10} \frac{\mathbb{E} [||\underline{d}_\tau||^2]}{\mathbb{E} [||\underline{d}_\tau - \hat{\underline{d}}_\tau||^2]} \quad (47)$$

with the noise-free observation estimate $\hat{\underline{d}}_\tau = \mathbf{C}_\tau \hat{\mathbf{w}}_{\tau-1}^{\text{kf}}$ (cf. Eq. (25)). Note that, in contrast to the system mismatch Υ_τ , the ERLE \mathcal{E}_τ represents a signal-dependent performance measure and, thus, is of particular interest for signal cancellation applications. The expectation operator $\mathbb{E}[\cdot]$ in Eq. (47) is here approximated by recursive averaging over time. To allow for more general conclusions, the system mismatch Υ_τ and the ERLE \mathcal{E}_τ are averaged over 50 trials of the random experiment with randomly chosen excitation signals, random microphone positions and random interfering noise signals. The respective averaged performance measures are denoted by an overbar ($\bar{\cdot}$).

In the following experiments we evaluate the proposed KF-ASP algorithm (cf. Alg. 1) for the previously described OSASI scenario. As baseline we use the state-of-the-art KF [27] (cf. Sec. 4.1) with a state transition factor $A = 0.9999$, a frame shift $R = 512$, a filter length $L = 512$ and recursive averaging factors $\lambda_W = 0.9$ and $\lambda_N = 0.5$. The state uncertainty matrix \mathbf{P}_τ (cf. Eq. (24)) was initialized with an identity matrix scaled by $P_0 = 0.01$. For the proposed algorithm we investigate three variants: KF-ASP (d_{kf} , Proj.), KF-ASP (d_{kf} , Comb.) and

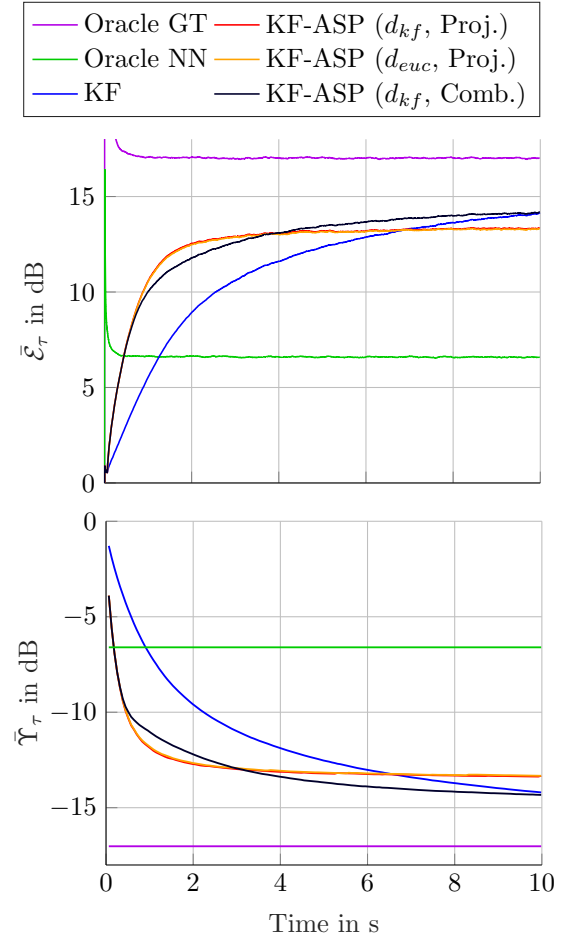


Figure 6 Evaluation of the proposed KF-ASP-based algorithmic variants for a system identification application ($\text{SNR}_{\text{wgn}} = 0$ dB, $\text{SNR}_{\text{sp}} = \infty$ dB) with a spatially uncorrelated WGN excitation signal.

KF-ASP (d_{euc} , Proj.). Here, the variants including d_{kf} use the probabilistic quadratic distance (37) whereas the last one, labeled by d_{euc} , uses the quadratic Euclidean distance (20) to compute the $K_\tau = 80$ NN training samples for the update in time step τ (cf. Sec. 4.2). The training data set is composed of $K = 5000$ spatially uniformly distributed AIRs. Furthermore, we compare the effect of the convex combination-based enhancement (cf. Sec. 4.3), labeled by *Comb.*, in contrast to a hard projection, i.e., choosing $\alpha_{b,\tau,f} = 1$ in Eq. (44), which is labeled by *Proj.* For the model prior (cf. Eq. (46)) $\beta_{\text{pr}} = 5$ is chosen. The state uncertainty matrices of the ASP-based algorithms were initialized with a scaling factor of $P_0 = 0.1$. Note that this higher initial state uncertainty could not be used in the baseline KF as it led to divergence in our experiments. In addition, we evaluated two oracle baselines, i.e., Oracle GT and Oracle

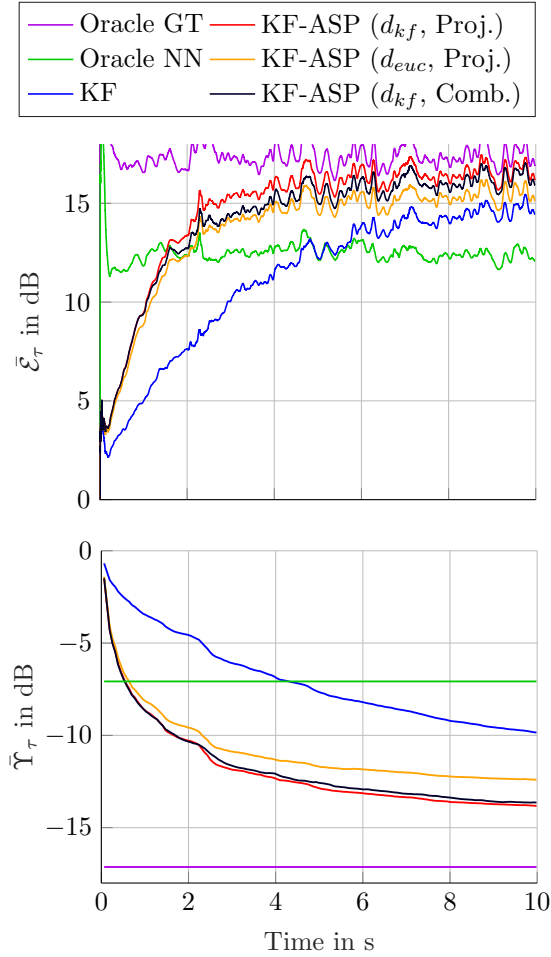


Figure 7 Evaluation of the proposed KF-ASP-based algorithmic variants for a system identification application ($\text{SNR}_{\text{wgn}} = 5$ dB, $\text{SNR}_{\text{sp}} = 0$ dB) with two independent speech excitation signals.

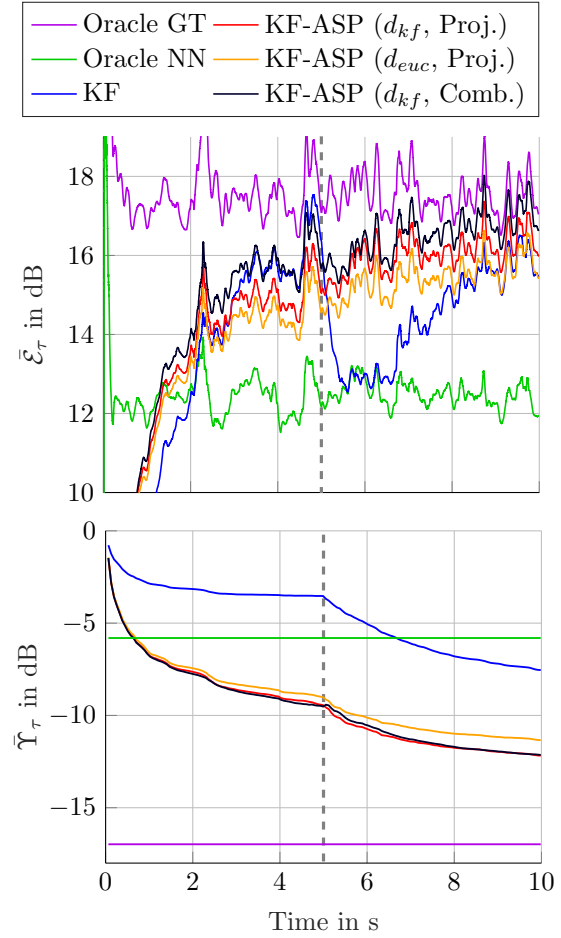


Figure 8 Evaluation of the proposed KF-ASP-based algorithmic variants for a teleconferencing setup ($\text{SNR}_{\text{wgn}} = 10$ dB, $\text{SNR}_{\text{sp}} = \infty$ dB). After 5 s the far-end speakers switch (indicated by a dashed gray line).

NN. Here, Oracle GT uses the first L taps of the true AIRs in \underline{w}_τ as estimate $\hat{\underline{w}}_\tau$ and Oracle NN the training sample with the smallest squared Euclidean distance (20) to the true AIR vector.

Fig. 6 shows the average ERLE $\bar{\mathcal{E}}_\tau$ and system mismatch $\tilde{\Upsilon}_\tau$ for an excitation with spatially uncorrelated stationary WGN input signal ($\text{SNR}_{\text{wgn}} = 0$ dB, $\text{SNR}_{\text{sp}} = \infty$ dB). We conclude from Fig. 6 that the proposed KF-ASP algorithms significantly increase the convergence rate of the baseline KF. However, the steady-state performance of the variants KF-ASP (d_{euc} , Proj.) and KF-ASP (d_{kf} , Proj.) which rely entirely on the hard projection, i.e., the choice $\alpha_{b,\tau,f} = 1$ in the convex combination (44), are significantly worse than the baseline KF. This is due to the imperfections of the affine subspace model whose modeling capability depends on the training sample size K and the choice of the subspace dimension D_τ (cf. Fig. 4). In

contrast, the soft projection-based KF-ASP approach (cf. Sec. 4.3) achieves an increased steady-state performance in comparison the hard projection-based variants due to the convex combination (cf. Eq. (44)) which takes the uncertainty of the model into account. Yet, the baseline KF still shows a slightly improved steady-state performance which motivates an adaptive control of the prior covariance matrix (46). Furthermore, we observe that the probabilistic distance d_{kf} performs similarly to the Euclidean distance d_{euc} . This is explained by the stochastic properties of the excitation and noise signals which do not result in a nonuniform frequency-dependent weighting in Eq. (36). Finally, by inspecting the performance of the Oracle NN algorithm we conclude that the affine subspace models generalize better to AIRs in between the training data samples.

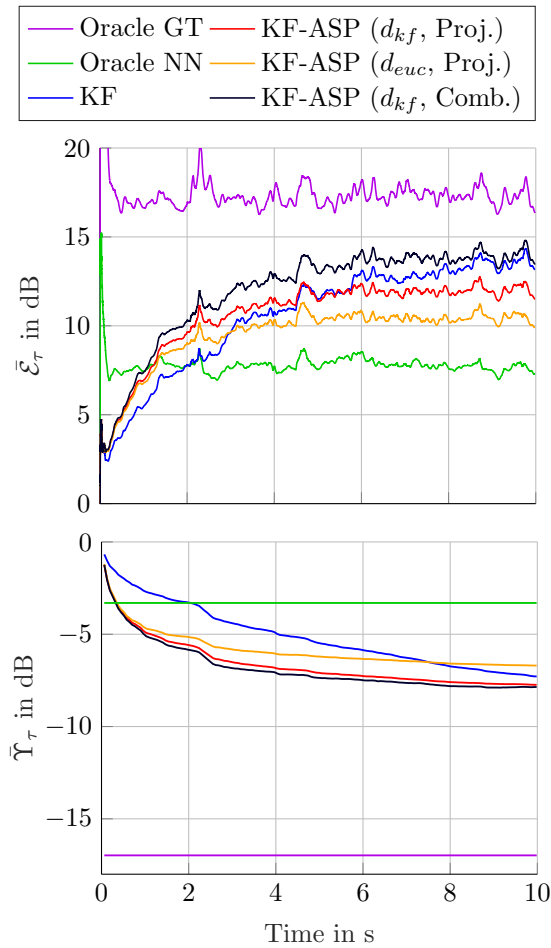


Figure 9 Evaluation of the proposed KF-ASP-based algorithmic variants for a training data size of $K = 1000$ samples. The loudspeakers play two independent speech signals ($\text{SNR}_{\text{wgn}} = 0$ dB, $\text{SNR}_{\text{sp}} = \infty$ dB).

A scenario with the two loudspeakers playing independent speech excitation signals is shown in Fig. 7 ($\text{SNR}_{\text{wgn}} = 5$ dB, $\text{SNR}_{\text{sp}} = 0$ dB). Similarly as for the WGN excitation the affine subspace projection greatly improves the convergence rate of the baseline KF. However, in contrast to the WGN excitation, the speech excitation benefits from the proposed probabilistic distance measure d_{kf} (37). This is explained by the nonuniform weighting in Eq. (36) which results from the frequency-dependent power of the speech excitation. Furthermore, the proposed KF-ASP algorithms show here an improved steady-state performance in comparison the KF baseline and almost achieve the Oracle GT performance.

We now extend the previous system identification scenarios to a typical acoustic echo cancellation (AEC) task in a teleconferencing setup ($\text{SNR}_{\text{wgn}} = 10$ dB, $\text{SNR}_{\text{sp}} = \infty$ dB). Here, we assume that the loud-

speaker array in the near-end room plays two microphone signals which are recorded in a distant far-end room [1]. The far-end microphone signals are composed of the reverberant speech signals of two spatially separated far-end speakers with disjoint activity. Due to the high spatial correlation of the recorded speech signals, the system identification in the near-end room is complicated by the nonuniqueness problem [25, 26]. Here, the near-end OSASI AEC algorithm can only estimate a nonunique cancellation filter which often leads to severe performance drops whenever the activity of the far-end speakers changes. Fig. 8 shows the average ERLE $\bar{\mathcal{E}}_\tau$ and system mismatch $\bar{\Upsilon}_\tau$ computed from 50 trials for the experiment. We conclude that, while the ERLE is high, the baseline KF does not converge towards the true AIRs. Due to the nonunique filter estimate the performance of the baseline KF significantly drops after the source activity switching at $t = 5$ s. In contrast, the KF-ASP-based algorithms achieve a much better average system mismatch $\bar{\Upsilon}_\tau$. This might be explained by the projections keeping the solution closer to the true AIR. Thus, there is no performance drop when the far-end speakers flip.

Finally, we evaluate the effect of the training data size K . To this end, we simulate an additional scenario with spatially uncorrelated speech excitation ($\text{SNR}_{\text{wgn}} = 0$ dB, $\text{SNR}_{\text{sp}} = \infty$ dB). However, in contrast to the previous experiments ($K = 5000$), the affine subspace models are learned from a training data set including only $K = 1000$ samples. The results shown in Fig. 9 suggest a rapidly decreasing performance of the algorithms relying on hard projection onto affine subspaces. This is explained by the reduced number of training data samples K which only allow to learn coarse AIR models. In contrast, the soft projection-based approach, which does not enforce that all AIR estimates are confined to the subspace model, still achieves an excellent steady-state performance in addition to the improved convergence rate.

6 Summary and Outlook

In this paper we have introduced a family of novel OSASI algorithms which exhibit significantly faster convergence properties and improved steady-state performance in scenarios suffering from high-level interfering noise and nonuniqueness of optimum filter estimates. The proposed algorithms assume that the variability of AIRs in an acoustic scene is confined to a non-linear manifold which can locally be approximated by an affine subspace. This allows to enhance an AF-based AIR estimate by projecting it onto the learned subspace. As future research we plan to develop improved choices for the prior covariance matrix and evaluate the effect of noisy training data samples on the learned AIR models.

Author details

Multimedia Communications and Signal Processing,
Friedrich-Alexander-University Erlangen-Nürnberg (FAU), Cauerstr. 7,
91058, Erlangen, Germany.

References

- G. Enzner et al., "Acoustic Echo Control," in *Academic Press Library in Signal Processing*, vol. 4, pp. 807–877. Elsevier, 2014.
- P. S. R. Diniz, *Adaptive Filtering: Algorithms and Practical Implementation*, Springer, Berlin, Heidelberg, 2007.
- B. Widrow and M. E. Hoff, "Adaptive Switching Circuits," in *WESCON Convention Record*, Los Angeles, USA, Aug. 1960, pp. 96–104.
- E. Ferrara, "Fast implementations of LMS adaptive filters," *Transactions on Acoustics, Speech, and Signal Processing*, vol. 28, no. 4, pp. 474–475, Aug. 1980.
- J. Benesty et al., "A Nonparametric VSS NLMS Algorithm," *IEEE Signal Processing Letters*, vol. 13, no. 10, pp. 581–584, 2006.
- F. Kuech et al., "State-space architecture of the partitioned-block-based acoustic echo controller," in *International Conference on Acoustics, Speech and Signal Processing (ICASSP)*, Florence, Italy, May 2014, pp. 1295–1299.
- S. Haykin, *Adaptive Filter Theory*, Prentice Hall, NJ, USA, 2002.
- E. Hänsler and G. Schmidt, *Acoustic Echo and Noise Control: A practical Approach*, Wiley-Interscience, NJ, USA, 2004.
- D. Mansour and A. Gray, "Unconstrained frequency-domain adaptive filter," *Transactions on Acoustics, Speech, and Signal Processing*, vol. 30, no. 5, pp. 726–734, Oct. 1982.
- J. Benesty and others., "A new class of doubletalk detectors based on cross-correlation," *IEEE Transactions on Speech and Audio Processing*, vol. 8, no. 2, pp. 168–172, Mar. 2000.
- B. H. Nitsch, "A frequency-selective stepfactor control for an adaptive filter algorithm working in the frequency domain," *Signal Processing*, vol. 80, no. 9, pp. 1733–1745, 2000.
- G. Enzner and P. Vary, "Frequency-domain adaptive Kalman filter for acoustic echo control in hands-free telephones," *Signal Processing*, vol. 86, no. 6, pp. 1140–1156, June 2006.
- S. Malik and G. Enzner, "Online maximum-likelihood learning of time-varying dynamical models in block-frequency-domain," in *International Conference on Acoustics, Speech and Signal Processing (ICASSP)*, Dallas, USA, Mar. 2010.
- C. Huemmer et al., "The NLMS algorithm with time-variant optimum stepsize derived from a bayesian network perspective," *IEEE Signal Processing Letters*, vol. 22, no. 11, pp. 1874–1878, 2015.
- F. Yang et al., "Frequency-Domain Adaptive Kalman Filter With Fast Recovery of Abrupt Echo-Path Changes," *IEEE Signal Processing Letters*, vol. 24, no. 12, pp. 1778–1782, Dec. 2017.
- T. Haubner et al., "Noise-robust adaptation control for supervised acoustic system identification exploiting a noise dictionary," in *accepted for International Conference on Acoustics, Speech and Signal Processing (ICASSP)*, Toronto, CA, June 2021.
- T. Haubner et al., "A synergistic kalman- and deep postfiltering approach to acoustic echo cancellation," 2020, [arXiv preprint:2012.08867, Dec. 2020].
- M. Fozunbal et al., "Multi-Channel Echo Control by Model Learning," in *International Workshop on Acoustic Echo and Noise Control (IWAENC)*, Seattle, USA, Sept. 2008.
- T. Koren et al., "Supervised system identification based on local PCA models," in *International Conference on Acoustics, Speech and Signal Processing (ICASSP)*, Kyoto, Japan, Mar. 2012.
- R. Talmon and S. Gannot, "Relative transfer function identification on manifolds for supervised GSC beamformers," in *European Conference on Signal Processing (EUSIPCO)*, Marrakech, Morocco, Sept. 2013.
- T. Haubner et al., "Online supervised acoustic system identification exploiting prelearned local affine subspace models," in *International Workshop on Machine Learning for Signal Processing (MLSP)*, Sept. 2020, pp. 1–6.
- B. Laufer-Goldshtein et al., "A Study on Manifolds of Acoustic Responses," in *Latent Variable Analysis and Signal Separation (LVA/ICA)*, Liberec, Czech Republic, Aug. 2015.
- R. Talmon et al., "Diffusion Maps for Signal Processing: A Deeper Look at Manifold-Learning Techniques Based on Kernels and Graphs," *IEEE Signal Processing Magazine*, vol. 30, no. 4, pp. 75–86, July 2013.
- I. T. Jolliffe, "Principal components in regression analysis," in *Principal component analysis*, pp. 129–155. Springer, 1986.
- M. M. Sondhi et al., "Stereophonic acoustic echo cancellation-an overview of the fundamental problem," *IEEE Signal Processing Letters*, vol. 2, no. 8, pp. 148–151, Aug. 1995.
- J. Benesty et al., "A better understanding and an improved solution to the specific problems of stereophonic acoustic echo cancellation," *IEEE Transactions on Speech and Audio Processing*, vol. 6, no. 2, pp. 156–165, Mar. 1998.
- S. Malik and G. Enzner, "Recursive Bayesian Control of Multichannel Acoustic Echo Cancellation," *IEEE Signal Processing Letters*, vol. 18, no. 11, pp. 619–622, Nov. 2011.
- L. W. Tu, *An Introduction to Manifolds*, Universitext. Springer New York, 2010.
- G. Strang, *Linear Algebra and its Applications*, Thomson, Brooks/Cole, Belmont, CA, 2006.
- S. Lloyd, "Least squares quantization in PCM," *IEEE Transactions on Information Theory*, vol. 28, no. 2, pp. 129–137, Mar. 1982.
- D. Arthur and V. Vassilvitskii, "K-means++: The advantages of careful seeding," in *Proceedings of the 18th Annual ACM-SIAM Symposium on Discrete Algorithms*, New Orleans, USA, 2007.
- C. M. Bishop, *Pattern Recognition and Machine Learning (Information Science and Statistics)*, Springer, Berlin, Heidelberg, 2007.
- H. Buchner et al., "Generalized multichannel frequency-domain adaptive filtering: efficient realization and application to hands-free speech communication," *Signal Processing*, vol. 85, no. 3, pp. 549–570, Mar. 2005.
- J. Franzen and T. Fingscheidt, "Improved Measurement Noise Covariance Estimation for N-channel Feedback Cancellation Based on the Frequency Domain Adaptive Kalman Filter," in *International Conference on Acoustics, Speech and Signal Processing (ICASSP)*, Brighton, UK, May 2019, pp. 965–969.
- K. B. Petersen and M. S. Pedersen, "The matrix cookbook," Nov. 2012, Version 20121115.
- J. B. Allen and D. A. Berkley, "Image method for efficiently simulating small-room acoustics," *Journal of the Acoustical Society of America*, vol. 65, no. 4, pp. 943–950, 1979.
- E. Habets, "Room Impulse Response Generator," Tech. Rep., Technische Universiteit Eindhoven, Sept. 2010.
- L. M. Panfili et al., "The UW/NU corpus, version 2.0," <https://depts.washington.edu/phonlab/projects/uwnu.php>, 2017.